Effect of Hydrogen on the Internal Oxidation of a Pd–Cr Alloy in Dual-Atmosphere Conditions

Downloaded from: https://research.chalmers.se, 2025-05-17 12:15 UTC

Citation for the original published paper (version of record):

Chyrkin, A., Cossu, C., Svensson, J. et al (2022). Effect of Hydrogen on the Internal Oxidation of a Pd–Cr Alloy in Dual-Atmosphere Conditions. Oxidation of Metals, 97(5-6): 527-538. http://dx.doi.org/10.1007/s11085-022-10104-8

N.B. When citing this work, cite the original published paper.

research.chalmers.se offers the possibility of retrieving research publications produced at Chalmers University of Technology. It covers all kind of research output: articles, dissertations, conference papers, reports etc. since 2004. research.chalmers.se is administrated and maintained by Chalmers Library

(article starts on next page)

Oxidation of Metals
https://doi.org/10.1007/s11085-022-10104-8

ORIGINAL PAPER

Effect of Hydrogen on the Internal Oxidation of a Pd–Cr Alloy in Dual-Atmosphere Conditions

Anton Chyrkin[1] · Camilla Cossu[1] · Jan-Erik Svensson[1] · Jan Froitzheim[1]

Received: 21 October 2021 / Revised: 23 February 2022 / Accepted: 24 February 2022
© The Author(s) 2022

Abstract

The effect of hydrogen on oxygen permeability has been studied in a diluted Pd–Cr alloy in dual- and single- atmosphere conditions between 600 and 950 °C. The 0.3 mm thick Pd–1.5Cr foil was exposed in dry and humid air as well as in dual-atmosphere conditions, with one sample surface being exposed to air and one to hydrogen, as encountered in solid oxide fuel cells. At all temperatures, Cr oxidized internally forming internal oxidation zones which were measured in metallographic cross sections. Below 800 °C, an external layer of PdO formed on the surface decreasing the internal oxidation kinetics. No measurable effect of hydrogen on the internal oxidation of Cr in Pd has been detected.

Keywords Internal oxidation · Hydrogen · Oxygen permeability · Palladium · Chromium · Dual atmosphere · SOFC

Introduction

High-temperature metallic materials are often applied in aggressive environments and rely for their corrosion resistance on the formation of compact, slow-growing, adherent, protective external oxide scales, Cr_2O_3 and/or α-Al_2O_3. It is well known that chromia-forming alloys perform worse in humid [1–4] and reducing H_2/H_2O [5, 6] gases. The presence of water vapor in both high and low oxygen potential atmospheres alters the scaling mechanism accelerating chromia growth [1, 3], promotes reactive evaporation and thus depletion of Cr [7–9], thereby undermining protectivity of the Cr_2O_3 scale [2, 4, 6, 10–12].

The detrimental effect of water vapor is often attributed to hydrogen dissolved in metal, which has been confirmed by the dual-atmosphere effect reported in solid oxide fuel cell (SOFC) literature [13–18]. In SOFC, the metallic

✉ Jan Froitzheim
jan.froitzheim@chalmers.se

[1] Chalmers Tekniska Hogskola, Gothenburg, Sweden

Published online: 28 March 2022

interconnect, commonly a sheet of ferritic stainless steel, is placed between individual cells connected to a fuel cell stack. While electrically connecting neighboring cells, it separates the fuel gas compartment (anode side) of one cell from the air compartment (cathode side) of the other cell. The interconnect is thus exposed to both environments in parallel, a situation described as dual atmosphere. Previous research has found evidence that in dual-atmosphere experiments hydrogen permeates a thin foil specimen and causes unprotective scaling or even the breakdown of pre-formed Cr_2O_3 scales [14, 15, 18–20].

The abundant studies on the role of hydrogen on the chromia scaling process have resulted in several proposed mechanisms: (1) water vapor promotes oxygen transport in the pores of the oxide bridging the voids [21]; (2) hydrogen alters the lattice point defect structure of Cr_2O_3 through incorporation of H^+ and/or HO^- into the scale [22] and thereby accelerates chromia growth [3, 19, 24]; (3) gas-transport reactions [4, 23] or Cr-oxyhydroxides [7]; iv) preferential adsorption of water molecules [4]; (4) hydrogen affects the morphology of internal oxidation and thus permeability [24]; and (5) dissolved hydrogen increases oxygen permeability, i.e., product of oxygen solubility and diffusivity, in the alloy, thus promoting internal oxidation, excessive composition of Cr and the earlier onset of breakaway oxidation [2, 5, 25–28].

As the SOFC interconnect is fully saturated with hydrogen permeating from the fuel side, the latter mechanism may play a key role in interpreting the dual-atmosphere effect. However, numerous authors have recently questioned the effect of water vapor and hydrogen on oxygen permeability when studying internal oxidation in Fe–Ni–Cr [29–31] and Pd–Cr [32] alloys. The aforementioned studies were carried out at temperatures that substantially exceed the application range of SOFC, 600–800 °C, while the dual-atmosphere effect has been shown to intensify with decreasing temperature [15]. Therefore, extrapolating the conclusions from [29–31] to lower temperatures must be done with the utmost precaution.

In a classical dual-atmosphere setup, i.e., humid air versus Ar–H_2–H_2O, it is impossible to study internal oxidation of Cr on the air side due to the rapid growth of iron-rich oxides. This experimental obstacle can be circumvented by using a model alloy in which the base metal oxidizes slowly in the given conditions or does not oxidize at all. Such a noble metal could be Pt or Pd. Pd–Cr alloys are known to form extremely distinct and uniform internal oxidation zones (IOZ) with a sharp interface that allows estimations of oxygen permeability in Pd with high precision [32, 33]. With a high solubility for oxygen [33, 34] and especially hydrogen [35–37], palladium is an excellent base metal to verify the effect of hydrogen in the dual-atmosphere experiment on the kinetics of internal oxidation in Pd. It is worth noting that palladium is not a structural material and the conclusion drawn in the present study should be interpreted with caution with respect to commercial Ni/Fe-base systems.

In the present paper, the effect of hydrogen on internal oxidation in Pd–Cr alloys in dual-atmosphere conditions has been studied. Oxygen permeability was measured for a Pd–1.5% (at.) Cr alloy in dry and humid lab air as well as dual-atmosphere conditions, i.e., air/Ar-H_2-H_2O, in the 600–950 °C temperature range.

Experimental Procedures

The diluted Pd–Cr alloy containing 1.5 at% Cr was produced by argon arc melting of high-purity metals (Pd 99.998% and Cr 99.99%) by HMW Hauner GmbH (Röttenbach, Germany). The alloy was supplied as a 0.3 mm thick foil.

The alloy coupons for single atmosphere exposures measuring 10 mm × 10 mm were cut from the foil while the circular specimens of 21 mm diameters were punched for dual-atmosphere exposures. The surfaces were not treated and remained as-rolled. The specimens were degreased with acetone and ethanol in an ultrasonic bath immediately prior to exposure.

The single atmosphere (air on both sides) exposures were carried out in horizontal tube furnaces at 600–950 °C for up to 192 h. To estimate the effect of PdO evaporation, the exposures at 600 and 700 °C were run in still dry air as well as in humid air with 3% H_2O at 6000 sml min^{-1} flow rate. The specimens were introduced directly into the hot zone of the furnace and removed rapidly after the exposure. The specimens were air-cooled. The specimens were weighed before and after exposure with a Mettler Toledo XP6 microbalance.

For the dual-atmosphere exposures, the disk specimens were mounted in a specimen holder made of 253 MA steel. Details on the dual-atmosphere setup can be found elsewhere [18]. Gold gaskets were used as a sealant to ensure that the system was gastight. The gas composition was Ar–5% H_2 + 3% H_2O with a flow rate of 100 sml min^{-1} on the simulated fuel side, while filtered laboratory air + 3% H_2O with a flow rate of 8800 sml min^{-1} was set for the air side. A heating/cooling rate of 1 °C min^{-1} was used for all exposures.

The exposed specimens were sectioned and mounted in resin for metallographic preparation. The cross sections were ground with sandpaper, polished with diamond paste to 0.25 µm surface finish, and analyzed with the optical microscope Zeiss Axio Observer. The IOZs were optically visible only in the 900 and 950 °C specimens. The polished cross sections were etched for 30–60 s with concentrated hydrochloric acid to get the optimum visual contrast between the IOZ and unreacted alloy. The SEM was performed to (1) better visualize IOZ without etching, (2) make sure that the IOZ morphologies previously reported in [32, 33] were reproduced in the present experiments and (3) confirm the IOZ depth measured using optical microscopy.

A Leica TIC 3X broad ion beam (BIB) instrument was used for the preparation of cross sections for scanning electron microscopy (SEM). Zeiss LEO Ultra FE-55 equipped with an in-lens detector, JEOL Prime and FEI Versa 3D Dual Beam were used for SEM imaging of the IOZs and the precipitates in them.

Results

Figure 1 shows the optical micrographs of the Pd-Cr alloy after single- (a) and dual-atmosphere (b) exposures at 900 °C for 8 h. The air-exposed foil specimen has internal oxidation zones (IOZs) on both sides, while in the

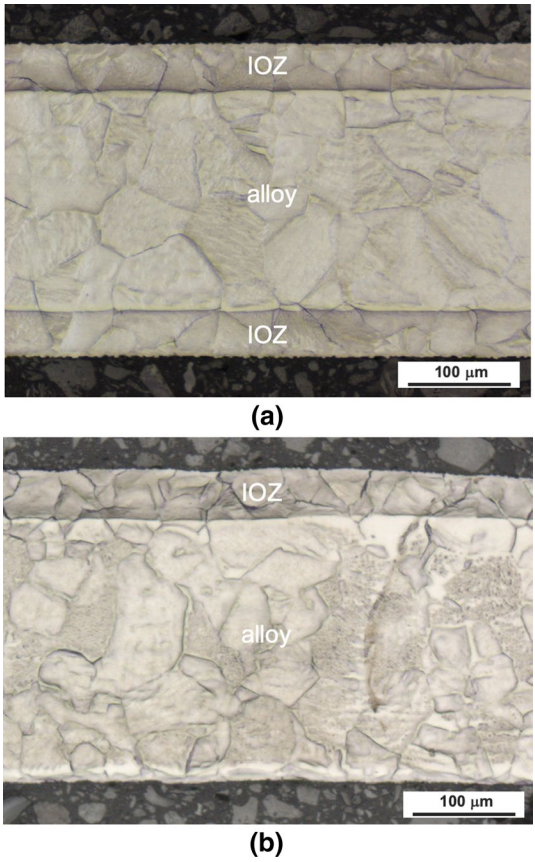

Fig. 1 Optical micrographs of etched cross sections of Pd–Cr alloy after exposure in single (**a**) and dual (**b**) atmosphere for 8 h at 900 °C

dual-atmosphere specimen, the IOZ is observed only on the air side where pO_2 was high. The change from ambient oxygen pressure (0.2 bar) to the pO_2 of the Ar-5%H_2–3%H_2O mixture at 900 °C (2×10^{-17}) will result in an IOZ that should be 10,000 times thinner than that in air, i.e., less than a micron. The IOZs in both samples (the air side in the dual atmosphere specimen) are approximately 50 μm thick.

The BSE images in Fig. 2 compare the IOZs in the single- (a) and the air side of dual-atmosphere (b) Pd–Cr specimens exposed at 900 °C for 8 h. In both cases, no external PdO scale has been detected. The IOZ consists of nano-dispersed precipitates of Cr_2O_3 (Fig. 2c, d) along with larger Cr_2O_3 precipitates at grain boundaries. The interface between the IOZ and unreacted alloy is sharp and straight.

Figure 3 shows the BSE micrographs of the BIB cross sections of the Pd–Cr alloy specimens exposed in single and dual atmosphere at 600 °C for 168 h. At the lower temperature, an external PdO scale can be observed on both specimens. PdO formation is expected at temperatures below 810 °C (the thermodynamics of PdO formation will be discussed in more detail below). Formation and vaporization of PdO resulted in moderate porosity in the near-surface region. The mass

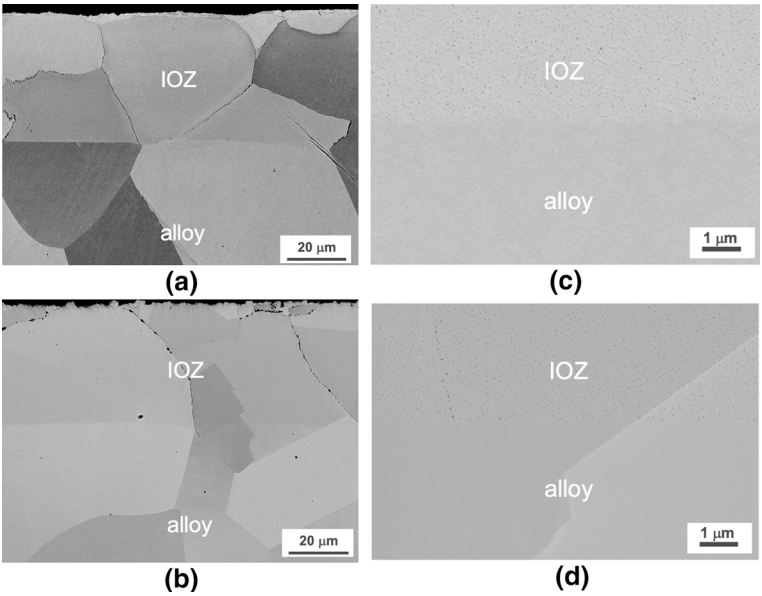

Fig. 2 BSE images of IOZ in Pd–Cr alloy after exposures in single (**a**, **c**) and dual (**b**, **d**) atmosphere for 8 h at 900 °C

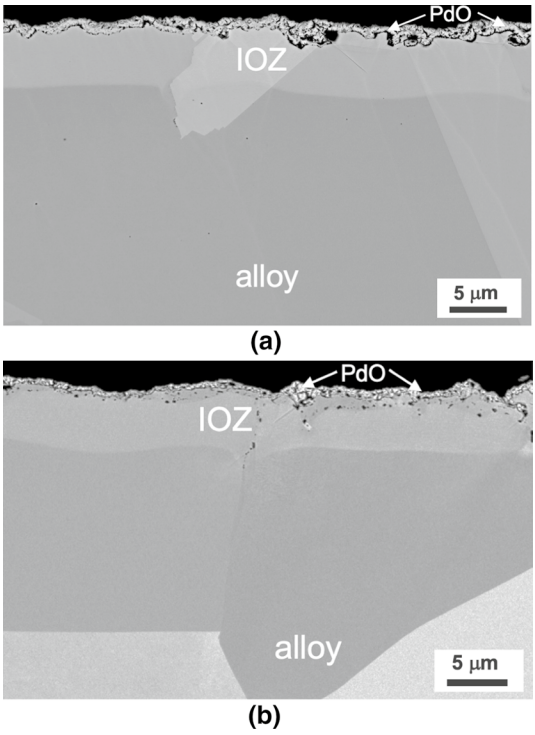

Fig. 3 BSE images of IOZ in Pd–Cr alloy after exposures in single (**a**) and dual (**b**) atmosphere for 168 h at 600 °C

loss due to PdO vaporization was limited. For example, the oxygen uptake by the Pd–Cr alloy exposed at 700 °C for 168 h in still dry air and in the high-flow humid air were 0.25 and 0.22 mg/cm^2, respectively. The difference was less pronounced and virtually negligible at higher temperatures. The IOZs were not affected by PdO vaporization.

The IOZ measurements are summarized in the kinetics plot in Fig. 4. The IOZ thicknesses in single and dual atmosphere were measured at four different temperatures (600–900 °C). The internal oxidation kinetics are parabolic and controlled by diffusion of oxygen. The single-atmosphere exposures were characterized by high precision and reproducibility. The IOZs measured in the dual-atmosphere conditions fall within the linear fits for the single atmosphere specimens and thus reveal no effect of dual atmosphere and, hence, dissolved hydrogen on the width of the internal oxidation zone in Pd–Cr.

Oxygen permeabilities $N_O^{(s)}D_O$ were calculated from the parabolic rate constants k_p^{IOZ} and plotted as a function of reciprocal temperature in Fig. 5 along with the available literature data. The $N_O^{(s)}D_O$ values are in very good agreement with the data by Gegner [33] and Shemet [32] above 800 °C. To the best of the authors' knowledge, there is no available experimental data in literature on oxygen permeability in palladium below PdO. Therefore, the data below 800 °C cannot be compared with any literature source. However, the low temperature $N_O^{(s)}D_O$ data is consistent and demonstrates higher temperature dependence and higher activation energy (202 kJ mol^{-1}) in comparison with the high-temperature regime (92 kJ mol^{-1}) without PdO above 800 °C.

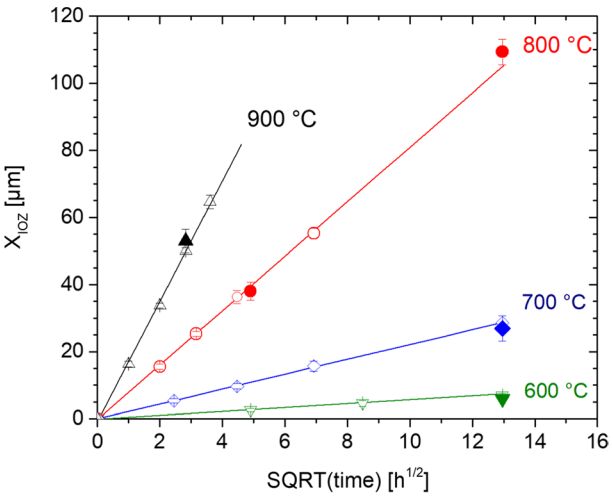

Fig. 4 Parabolic kinetics of IOZ growth in Pd–Cr alloy in single (empty symbols) and dual atmosphere (full symbols) at 600–900 °C

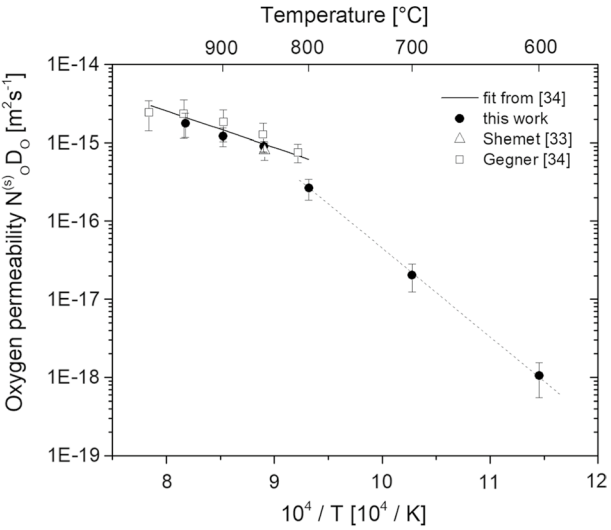

Fig. 5 Temperature dependence of oxygen permeability in palladium: comparison with literature data

Discussion

Oxygen Permeability in Palladium

Internal oxidation in palladium is governed by diffusion of oxygen [32, 33], has parabolic kinetics, and obeys the following time law:

$$X_{\mathrm{IOZ}}^2 = 2k_{\mathrm{p}}^{\mathrm{IOZ}} t \tag{1}$$

where X_{IOZ} is the IOZ width in m, $k_{\mathrm{p}}^{\mathrm{IOZ}}$ is the parabolic rate constant in $\mathrm{m}^2\ \mathrm{s}^{-1}$, and t is time in s. The parabolic rate constant of internal oxidation is directly related to oxygen permeability [38].

$$k_{\mathrm{p}}^{\mathrm{IOZ}} = \frac{N_{\mathrm{O}}^{(\mathrm{s})} D_{\mathrm{O}}}{\nu N_{\mathrm{Cr}}} \varepsilon \tag{2}$$

Here, the product $N_{\mathrm{O}}^{(\mathrm{s})} D_{\mathrm{O}}$ is the oxygen permeability, where $N_{\mathrm{O}}^{(\mathrm{s})}$ is the equilibrium oxygen solubility in metal in terms of mole-fraction and D_{O} is oxygen diffusivity $\mathrm{m}^2\ \mathrm{s}^{-1}$. ν is the stoichiometric ratio O/Cr in the precipitated oxide (1.5 for chromia), N_{Cr} is the mole-fraction of Cr in the alloy and ε is a tortuosity factor accounting for the diffusion blocking effect of the oxide precipitates. For Pd–Cr alloys with the finely dispersed, equiaxed Cr_2O_3 precipitates, ε is considered to be unity [32, 33]. For Eq. (2) to be valid, the inward oxygen flux must significantly exceed the outward Cr diffusion, i.e., $N_{\mathrm{O}}^{(\mathrm{s})} D_{\mathrm{O}} \gg N_{\mathrm{Cr}} D_{\mathrm{Cr}}$, which was demonstrated by diffusion analysis in [32].

The oxygen permeabilities were computed using Eq. (2) and compared with the available literature data [32, 33]. The oxygen permeabilities measured above 800 °C are in excellent agreement with the data from [32, 33]. The data by Park and Altstetter [39] were ignored. As demonstrated by Gegner et al. [33], the oxygen solubility data in [39] obtained by coulometric titration were orders of magnitude lower than their own measurements and those in [34]. Considering this high discrepancy between the aforementioned two datasets and unknown source of the discrepancy, only the $N_O^{(s)} D_O$ data obtained by the internal oxidation technique are presented in and shown in Fig. 5.

Below 800 °C there is no available data for the oxygen permeabilities in palladium equilibrated with PdO. Below 800 °C, the activation energy increases from 92 to 202 kJ mol^{-1}, which will be discussed in the following section.

External PdO Scale

Apart from extremely high solubility for hydrogen as well as distinct and easily measurable IOZs in diluted Pd–Cr alloys, the absence of external oxide is one of the reasons to choose Pd as the base metal for internal oxidation studies [32, 33]. However, Pd is known to oxidize at lower temperatures, forming a volatile oxide PdO [40, 41]. According to [33], the decomposition oxygen partial pressure of PdO can be given by the following expression:

$$p^*_{O_2} = 1.91 \times 10^{10} \exp\left(\frac{2\Delta H_{PdO}}{RT}\right) \tag{3}$$

where $p^*_{O_2}$ is the oxygen partial pressure in bar, ΔH_{PdO} is the enthalpy of formation for PdO ranging in the literature from − 112 [42, 43] to − 119 [44] kJ mol^{-1}, and R is the gas constant.

According to Eq. (3), $p^*_{O_2}$ (PdO) reaches the atmospheric partial pressure of 0.2 bar at 810 °C, which is close to the experimentally established decomposition temperature T_d ranging from 810 to 814 °C [40, 41]. Therefore, most previous internal oxidation studies were carried out either at elevated temperatures or at lower oxygen partial pressures to avoid PdO formation [32, 33, 45, 46].

In practical terms, exposures below 800 °C will have the following implications for the Pd–Cr alloy: (1) external PdO scale above the IOZ, (2) shallower IOZs as the oxygen solubility $N_O^{(s)}$ will be set by the Pd/PdO equilibrium partial pressure and not the atmospheric one, and (3) porosity due to volatilization of PdO. All three phenomena were experimentally observed. The external PdO scales were found on the specimens exposed in both dual and single atmosphere at 600 and 700 °C, with the IOZs being narrow and porous (Fig. 3). Pd evaporation was detected in a very little mass loss of the specimens in high-flow wet exposures. The difference between dry and wet mas gain was 0.04 mg/cm^2 after 192 h at 700 °C which corresponds to 0.05 µm of the metal loss. Given the IOZ widths, tens of µms (see Fig. 4), Pd evaporation was concluded not to affect internal oxidation. A separate series of exposures

in stagnant dry air revealed no effect of humidity and flow rate on IOZ thickness between high-flow humid air and stagnant dry air, as previously reported in [32].

The effect of PdO can be also seen in the temperature dependence of oxygen permeability (Fig. 5). Above 800 °C, the activation energy E_A for $N_O^{(s)}D_O$ was determined to be 92 kJ mol^{-1}, which is close to the value of 85 kJ mol^{-1} reported by Gegner et al. [33]. Combining the square-root dependence of oxygen solubility from oxygen partial pressure with Eq. (3), one arrives at the expression for activation energy for $N_O^{(s)}D_O$ below PdO: $E_A^* = E_A - \Delta H_{PdO}$. The predicted E_A^* for oxygen permeability underneath external PdO is 204 kJ mol^{-1}, which is in excellent agreement with the experimental value of 202 kJ mol^{-1}.

Effect of Hydrogen

Palladium is very well known for its extreme hydrogen solubility, especially at room temperature [35, 36, 47]. Hydrogen solubility in palladium is endothermic, i.e., the solubility N_H^{Pd} decreases with increasing temperatures. However, even at 500–1200 °C, the temperature range relevant for high-temperature corrosion, the amount of hydrogen dissolved by palladium is one to two orders of magnitude larger compared to iron or nickel [47]. For example, in the present study, the Pd–Cr alloy was in equilibrium with the gas containing 5% hydrogen. Using the original data by Sieverts [35, 36] and his solubility law, one arrives at $N_H^{Pd} = 1800$ at. ppm at 800 °C while $N_H^{Ni} = 135$ at. ppm [48] and $N_H^{Fe} = 45$ at. ppm [49] for these conditions, respectively.

The high solubility of hydrogen in Pd was the main motivation to explore its effect on oxygen permeability in the experiment by Shemet and Hänsel [32]. Comparing IOZs obtained in Pd–1Cr alloy exposed to dry and wet Ar–1%O_2 at 850 °C and the oxygen permeabilities derived from these experiments, the authors concluded that hydrogen had no effect on oxygen permeability in Pd. However, this conclusion was premature. The experiments confirmed no effect of water vapor but not necessarily no effect of hydrogen. The partial pressure of hydrogen can be calculated for the water decomposition reaction at 850 °C using the oxygen partial pressure, 1%, and the highest humidity level, 10%, in the work by Shemet and Hänsel. The resulting p_{H_2} is vanishingly small, 2.5×10^{-9} bar, and leads to an extremely low hydrogen solubility, $N_H^{Pd} = 0.5$ at. ppm, in palladium in equilibrium with a humid gas. Thus, the experiment in [32] proves only that there is no effect of humidity on $N_O^{(s)}D_O$ but does not allow a conclusion about any effect of hydrogen.

On the other hand, the dual-atmosphere experiment allows holding one side of the foil specimen in equilibrium with a hydrogen-containing gas, thus saturating Pd with hydrogen up to the equilibrium solubility on the level of 10^3 at. ppm. The immediate effect of hydrogen can be seen in Fig. 1: in the dual-atmosphere specimen, the IOZ formed only on the air side while the p_{O_2} in the H_2/H_2O gas mixture (e.g., $p_{O_2} = 2.1 \times 10^{-17}$ bar at 900 °C) was very low and, hence, $N_O^{(s)}D_O$ was so low. The oxygen solubility $N_O^{(s)}$ is eight orders of magnitude lower than that on the air side (0.2 bar) and thus the IOZ is virtually non-existent. Nor can PdO form at

such a low oxygen partial pressure [40]. Therefore, one may conclude that the Pd–Cr foil specimen was in equilibrium with hydrogen in the gas.

The micrographs in Figs. 1, 2 and 3 along with the IOZ kinetics plot in Fig. 4 provide compelling evidence of no effect of hydrogen on the IOZ width on the air side and, hence, the oxygen permeability $N_O^{(s)}D_O$ in palladium. No acceleration of internal oxidation has been observed in the entire temperature range of 600–900 °C relevant for the dual-atmosphere effect. No anomalous temperature dependence such as the one observed for the dual-atmosphere effect, most pronounced at 600 °C and alleviating with increasing temperature [14, 15], has been observed in the Pd–Cr alloy. Considering the exceptionally high hydrogen solubility in palladium, it is hard to imagine how dissolved hydrogen can affect $N_O^{(s)}D_O$ in iron or nickel in which the hydrogen solubility is a few orders of magnitude lower.

The latter assumption found numerous conformations in dedicated internal oxidation studies comparing the exposures in H_2/H_2O, CO/CO_2 and Rhines pack mixtures M/MO_x for Ni–Cr [31] and Ni–Fe–Cr alloys [29, 30]. Furthermore, the effect of hydrogen on internal oxidation can be indirectly studied in chromia-forming alloys exposed in air and H_2/H_2O. The elements with a higher affinity to oxygen, such as aluminum and titanium, tend to form IOZs underneath external chromia. No acceleration of internal oxidation can be deduced from the results demonstrated for either ferritic steels [50] or nickel-base alloys [51], especially in dual-atmosphere exposures [52]. However, a clear reservation needs to be made: all the afore-mentioned alloy systems have different lattice structures and thus cannot be directly compared between each other.

Conclusions

The dual-atmosphere exposures show no effect of hydrogen/humidity on the internal oxidation and, hence, oxygen permeability $N_O^{(s)}D_O$ in palladium in the entire temperature range. The dual-atmosphere experiment allows extreme saturations of the specimen with hydrogen while keeping the air side at high oxygen potential. Since the hydrogen effect on oxygen permeability is not detectable even in Pd exposed to a dual atmosphere, the hydrogen solubility reaching 1500–2000 at. ppm, it is very unlikely to expect it in the metals with much lower solubility for hydrogen such as iron or nickel.

The detrimental effect of hydrogen on selective oxidation of Fe–Cr alloys in humid oxidizing gases, H_2/H_2O and dual-atmosphere conditions must be attributed to another mechanism disrupting the chromium consumption–supply balance at the oxide–metal interface, e.g., scaling rate and/or Cr diffusion in metal.

Acknowledgements The authors are grateful for funding by the Swedish Energy Agency (Grant 2015-009652) and the Swedish High Temperature Corrosion Centre. This work was performed in part at the Chalmers Material Analysis Laboratory, CMAL.

Funding Open access funding provided by Chalmers University of Technology.

Open Access This article is licensed under a Creative Commons Attribution 4.0 International License, which permits use, sharing, adaptation, distribution and reproduction in any medium or format, as long as you give appropriate credit to the original author(s) and the source, provide a link to the Creative Commons licence, and indicate if changes were made. The images or other third party material in this article are included in the article's Creative Commons licence, unless indicated otherwise in a credit line to the material. If material is not included in the article's Creative Commons licence and your intended use is not permitted by statutory regulation or exceeds the permitted use, you will need to obtain permission directly from the copyright holder. To view a copy of this licence, visit http://creativecommons.org/licenses/by/4.0/.

References

1. D. J. Young, *Materials Science Forum* **595–598**, 1189 (2008).
2. E. Essuman, G. H. Meier, J. Żurek, M. Hänsel, and W. J. Quadakkers, *Oxidation of Metals* **69**, 143 (2008).
3. A. Galerie, J. P. Petit, Y. Wouters, J. Mougin, A. Srisrual, and P. Y. Hou, *Materials Science Forum* **696**, 200 (2011).
4. J. Ehlers, D. J. Young, E. J. Smaardijk, et al., *Corrosion Science* **48**, 3428 (2006).
5. W. J. Quadakkers, J. Żurek, and M. Hänsel, *JOM* **61**, 44 (2009).
6. D. J. Young, J. Żurek, L. Singheiser, and W. J. Quadakkers, *Corrosion Science* **53**, 2131 (2011).
7. H. Asteman, J. E. Svensson, and L. G. Johansson, *Oxidation of Metals* **57**, 193 (2002).
8. D. J. Young and B. A. Pint, *Oxidation of Metals* **66**, 137 (2006).
9. R. Sachitanand, M. Sattari, J.-E. Svensson, and J. Froitzheim, *International Journal of Hydrogen Energy* **38**, 15328 (2013).
10. B. Pujilaksono, T. Jonsson, H. Heidari, M. Halvarsson, J. E. Svensson, and L. G. Johansson, *Oxidation of Metals* **75**, 183 (2011).
11. G. H. Meier, K. Jung, N. Mu, et al., *Oxidation of Metals* **74**, 319 (2010).
12. J. Żurek, E. Wessel, L. Niewolak, et al., *Corrosion Science* **46**, 2301 (2004).
13. G. R. Holcomb, M. Ziomek-Horoz, S. D. Cramer, B. S. Covino, and S. J. Bullard, *Journal of Materials Engineering and Performance* **15**, 404 (2006).
14. K. O. Gunduz, A. Chyrkin, C. Goebel, et al., *Corrosion Science* **179**, 109112 (2021).
15. P. Alnegren, M. Sattari, J. E. Svensson, and J. Froitzheim, *Journal of Power Sources* **392**, 129 (2018).
16. K. Chandra and A. Kranzmann, *Corrosion Engineering, Science and Technology* **53**, 27 (2018).
17. C. Goebel, P. Alnegren, R. Faust, J. E. Svensson, and J. Froitzheim, *International Journal of Hydrogen Energy* **43**, 14665 (2018).
18. P. Alnegren, M. Sattari, J. E. Svensson, and J. Froitzheim, *Journal of Power Sources* **301**, 170 (2016).
19. Z. Yang, G. Xia, P. Singh, and J. W. Stevenson, *Solid State Ionics* **176**, 1495 (2005).
20. J. Rufner, P. Gannon, P. White, et al., *International Journal of Hydrogen Energy.* **33**, 1392 (2008).
21. A. Rahmel and J. Tobolski, *Corrosion Science* **5**, 815 (1965).
22. B. Tveten, G. Hultquist, and T. Norby, *Oxidation of Metals* **51**, 221 (1999).
23. T. Norby, *Le Journal de Physique IV* **3**, C9-99 (1993).
24. C. T. Fujii and R. A. Meussner, *Journal of the Electrochemical Society* **111**, 1215 (1964).
25. W. Zhao, Y. Kang, J. M. A. Orozco, and B. Gleeson, *Oxidation of Metals* **83**, 187 (2015).
26. E. Essuman, G. H. Meier, J. Zurek, M. Hänsel, L. Singheiser, and W. J. Quadakkers, *Scripta Materialia* **57**, 845 (2007).
27. J. Zurek, G. H. Meier, E. Wessel, L. Singheiser, and W. J. Quadakkers, *Materials and Corrosion* **62**, 504 (2011).
28. A. R. Setiawan, M. Hanafi Bin Ani, M. Ueda, K. Kawamura, and T. Maruyama, *ISIJ International* **50**, 259 (2010).
29. A. M. H. Bin, T. Kodama, M. Ueda, K. Kawamura, and T. Maruyama, *Materials Transactions* **50**, 2656 (2009).
30. D. Jullian, J. Zhang, D. B. Hibbert, and D. J. Young, *Journal of Alloys and Compounds* **732**, 646 (2018).

31. A. Prillieux, D. Jullian, J. Zhang, D. Monceau, and D. J. Young, *Oxidation of Metals* **87**, 273 (2017).
32. P. Guo, J. Zhang, D. J. Young, and C. H. Konrad, *Oxidation of Metals* **83**, 223 (2015).
33. V. Shemet and M. Hänsel, *Materials Letters* **172**, 6–10 (2016).
34. J. Gegner, G. Hörz, and R. Kirchheim, *Journal of Materials Science* **44**, 2198 (2009).
35. H. Jehn and E. Grallath, Solid solubility of oxygen in palladium, in *Precious Metals: Mining, Extraction, and Processing*, eds. V. Kudryk, D. A. Corrigan and W. W. Liang (TMS-AIME, Warrendale, 1984), pp. 595.
36. A. Sieverts and G. Zapf, *Zeitschrift für Phys. Chemie.* **174A**, 359 (1935).
37. A. Sieverts and G. Zapf, *Zeitschrift für Physikalische Chemie* **38B**, 46 (1938).
38. G. L. Holleck, *The Journal of Physical Chemistry* **74**, 503 (1970).
39. F. H. Stott and G. C. Wood, *Materials Science and Technology (United Kingdom)* **4**, 1072 (1988).
40. J. Park and C. J. Altstetter, *Scripta Metallurgica* **19**, 1481 (1985).
41. H. Zhang, J. Gromek, G. W. Fernando, S. Boorse, and H. L. Marcus, *Journal of Phase Equilibria* **23**, 246 (2002).
42. R. J. Farrauto, J. K. Lampert, M. C. Hobson, and E. M. Waterman, *Applied Catalysis B: Environmental* **6**, 263 (1995).
43. N. N. Smirnova, T. A. Bykova, N. A. Polotnyanko, N. D. Shikina, and I. L. Khodakovskii, *Russian Journal of Physical Chemistry A* **84**, 1851 (2010).
44. C. Mallika, O. M. Sreedharan, and J. B. Gnanamoorthy, *Journal of the Less Common Metals* **95**, 213 (1983).
45. J. Nell and H. S. C. O'Neill, *Geochimica et Cosmochimica Acta* **60**, 2487 (1996).
46. J. Gegner, *Israel Journal of Chemistry* **47**, 279 (2007).
47. A. S. Fjellvåg, D. Waller, J. Skjelstad, and A. O. Sjåstad, *Johnson Matthey Technology Review* **63**, 236 (2019).
48. H. Wipf, *Physica Scripta* **T94**, 43 (2001).
49. Y. Ebisuzaki, W. J. Kass, and M. O'Keeffe, *The Journal of Chemical Physics* **46**, 1378 (1967).
50. K. Kiuchi and R. B. McLellan, *Acta Metallurgica* **31**, 961 (1983).
51. J. P. Abelián, *ECS Proceedings Volumes* **2001–16**, 811 (2001).
52. A. Chyrkin, P. Huczkowski, V. Shemet, L. Singheiser, and W. J. Quadakkers, *Oxidation of Metals* **75**, 143 (2011).
53. A. W. B. Skilbred and R. Haugsrud, *International Journal of Hydrogen Energy* **37**, 8095 (2012).

Publisher's Note Springer Nature remains neutral with regard to jurisdictional claims in published maps and institutional affiliations.